Published in final edited form as:
Cell Stem Cell. 2013 February 7; 12(2): 252–264. doi:10.1016/j.stem.2012.12.002.

Human iPSC-derived oligodendrocyte progenitors can myelinate and rescue a mouse model of congenital hypomyelination

Su Wang[1], **Janna Bates**[1], **Xiaojie Li**[1], **Steven Schanz**[1], **Devin Chandler-Militello**[1], **Corri Levine**[1], **Nimet Maherali**[2], **Lorenz Studer**[3], **Konrad Hochedlinger**[2], **Martha Windrem**[1], and **Steven A. Goldman**[1,*]

[1]Center for Translational Neuromedicine and the Department of Neurology, University of Rochester Medical Center, Rochester, NY, 14642, USA

[2]Harvard Stem Cell Institute, 42 Church Street, Cambridge, MA, 02138, USA

[3]Developmental Biology Program, Sloan-Kettering Institute, 1275 York Ave., New York, NY, 10065, USA

Abstract

Neonatal engraftment by oligodendrocyte progenitor cells (OPCs) permits the myelination of congenitally dysmyelinated brain. To establish a potential autologous source of these cells, we developed a strategy by which to differentiate human induced pluripotential stem cells (hiPSCs) into OPCs. From 3 hiPSC lines, as well as from human embryonic stem cells (hESCs), we generated highly enriched OLIG2$^+$/PDGFRα$^+$/NKX2.2$^+$/SOX10$^+$ hOPCs, which could be further purified using fluorescence-activated cell sorting. hiPSC OPCs efficiently differentiated into both myelinogenic oligodendrocytes and astrocytes, in vitro and in vivo. Neonatally engrafted hiPSC OPCs robustly myelinated the brains of myelin-deficient shiverer mice, and substantially increased the survival of these mice. The speed and efficiency of myelination by hiPSC OPCs was higher than that previously observed using fetal tissue-derived OPCs, and no tumors from these grafts were noted as long as 9 months after transplant. These results suggest the utility of hiPSC-derived OPCs in treating disorders of myelin loss.

Keywords

glial progenitor cell; iPS cell; embryonic stem cell; neural stem cell; remyelination

A number of strategies have been developed for the cell-based repair of demyelinated lesions of both the brain and spinal cord (Ben-Hur and Goldman, 2008; Franklin and ffrench-Constant, 2008). In particular, human glial progenitor cells capable of oligodendrocytic maturation and myelination have been derived from both fetal and adult human brain tissue (Dietrich et al., 2002; Roy et al., 1999; Windrem et al., 2004), as well as from human embryonic stem cells (Hu et al., 2009b; Izrael et al., 2007b; Keirstead et al., 2005), and have proven effective in experimental models of both congenitally

*Address correspondence to: Steve Goldman, M.D., Ph.D., Center for Translational Neuromedicine, University of Rochester Medical Center, 601 Elmwood Rd., Box 645, Rochester, NY 14642, steven_goldman@urmc.rochester.edu, Phone: 585-275-9550, Fax: 585-276-2298.

dysmyelinated (Sim et al., 2011; Windrem et al., 2004; Windrem et al., 2008) and adult demyelinated (Windrem et al., 2002) brain and spinal cord. Yet these successes in immunodeficient mice notwithstanding, immune rejection has thus far hindered the use of allogeneic human cells as transplant vectors. Concern for donor cell rejection has been especially problematic in regards to the adult demyelinating diseases such as multiple sclerosis, in which the inflammatory processes underlying these disorders can present an intrinsically hostile environment to any allogeneic grafts (Keyoung and Goldman, 2007).

To address this issue, we sought to develop a robust protocol for the scalable production of myelinogenic oligodendrocytes from skin-derived human induced pluripotential cells (hiPSCs). By constructing hiPS cells from skin or blood derived from given patients, one may hope to generate sufficient OPCs to provide myelinogenic autografts, largely – though perhaps not completely - free of rejection risk. To this end, in this study we developed protocols by which we have generated highly-enriched populations of human OPCs, from multiple lines of both hiPSCs and hES cells. These cells reliably progress through serial stages of neural, glial progenitor cell and both oligodendrocytic and astrocytic differentiation in vitro. On that basis, we assessed the myelination competence of the hiPSC-derived OPCs (hiPSC OPCs) in a genetic model of congenital hypomyelination, the shiverer mouse, and established their ability to efficiently and robustly myelinate the hypomyelinated shiverer brain, with no evidence of either tumorigenesis or heterotopic non-glial differentiation. The transplanted animals survived significantly longer than their untreated counterparts, and the majority were frankly spared otherwise early lethality, a striking clinical rescue of a fatal hereditary disorder via an iPSC-based strategy. These data thus strongly support the utility of hiPSCs as a feasible and effective source of OPCs and their derived myelinogenic central oligodendrocytes, and suggest the potential of these cells as therapeutic vectors in disorders of central myelin.

RESULTS

Human iPSCs can be efficiently directed to glial progenitor cell fate

We used 4 different pluripotential stem cell lines from 3 different sources for this study; these included WA09/H9 hESC (Thomson et al., 1998); keratinocyte-derived K04 human iPS cells (Maherali et al., 2008); and fibroblast-derived C14 and C27 hiPSCs (Chambers et al., 2009). We selected specific features of several published protocols for the production of glial progenitor cells from hESC (Hu et al., 2009b; Izrael et al., 2007b), and then optimized the resultant hybrid protocol for use with WA09/H9 hESC cells. We then modified the resultant protocol to further optimize its efficiency with the 3 hiPSC cell lines, which were derived in different labs, from different cell sources, using different reprogramming protocols (Chambers et al., 2009; Maherali et al., 2008) (Figure S1). We found that the resultant 6-stage OPC differentiation protocol - which spans a range of 110-150 days in vitro as detailed in the Supplemental Methods and schematized in Figure 1 - efficiently generated hOPCs as well as their mature progeny, including both astrocytes and oligodendrocytes, from hESCs and hiPSCs alike (Figures 1B-1P). Its efficiency of OPC production, as defined by the incidence of $OLIG2^+/NKX2.2^+$ gliogenic (Qi et al., 2001; Zhou et al., 2001; Zhou et al., 2000) cell clusters in stage 6, ranged from 45.4 ± 20.3% in WA09/H9-derived hESCs to 73.8 ± 8.7%, 78.9 ± 6.1% and 79.5 ± 8.5% in K04-, C14- and C27-derived OPCs respectively (all data are provided as means ± SEM; Figures 2A and S2). Thus, each of the hiPSC and hES lines could be directed into highly enriched preparations of $OLIG2^+/PDGFR\alpha^+/NKX2.2^+/SOX10^+$ OPCs. Indeed, the efficiencies of OPC differentiation from hiPSCs, whether induced from keratinocytes (K04 cells) or fibroblasts (C14 and C27 cells), were consistently higher than that of WA9/H9 hES cells.

Both astrocytes and oligodendrocytes are efficiently derived from hiPSC-derived hOPCs

Both in vitro and in vivo, hiPSC OPCs readily differentiated into astrocytes as well as oligodendrocytes. GFAP-defined astroglia first appeared by 70 DIV, significantly earlier than did oligodendrocytes. By late stage 6 at 120 DIV, $GFAP^+$ astrocytes were found to be abundant when gliogenic spheres were plated onto polyornithine/laminin-coated surface (Figures 2B-2D). By that time, $GFAP^+$ cells comprised 40-50% of cells in OPC-induced cultures, across all cell lines (Figure 2D). Quantitative RT-PCR confirmed the upregulation of GFAP mRNA expression during OPC differentiation in all cell lines (Supplemental Table 1A).

The production of oligodendrocytes from hESC- and hiPSC-derived OPCs was triggered by the withdrawal of gliogenic growth factors to half-normal levels (see Methods). When hiPSC OPCs were exposed to those conditions for 2 weeks, a proportion matured into $O4^+$ and/or MBP^+ oligodendrocytes (Figures 2E-2G). By flow cytometry, $O4^+$ oligodendrocytes in C27, C14 and K04 hiPSC-derived OPC cultures respectively comprised 11.9 ± 3.8%, 4.1 ± 0.9%, and 7.6 ± 1.5% of all cells (at 194 ± 15, 186 ± 14 and 205 ± 14 DIV, respectively; means ± SEM) (Figure 3A, Supplementary Table 1B). Of note, our culture conditions favored initial oligodendrocytic differentiation but not post-mitotic oligodendrocytic survival, as our focus was on preparing populations of transplantable lineage-biased progenitors and immature oligodendroglia, rather than more mature – but less transplantable – process-bearing oligodendrocytes.

OPCs could be isolated from hiPSC cultures by CD140a- and CD9-directed FACS

Flow cytometry for A2B5, CD140a/PDGFαR and the tetraspanin CD9 (Berry et al., 2002; Terada et al., 2002) were next used to identify and quantify hiPSC OPCs in stage 6 culture (Figures 3B-C). $CD140a^+$ OPCs derived from C27, C14 and K04 hiPSCs respectively comprised 33.0 ± 10.3%, 32.8 ± 12.0%, and 41.1 ± 6.1% of all cells, compared to 37.5 ± 10.2% of H9-derived cells (Figure 3C, Supplementary Table 1C). The $CD9^+$ fraction of $CD140a^+$ cells, which defined a later-stage pool of OPCs, comprised 24.0 ± 8.0% and 12.4 ± 2.3% of cells in stage 6 C27 and K04 hiPSC cultures, respectively; matched cultures of H9-derived OPCs included 15.0 ± 4.9% $CD9^+/CD140a^+$ cells (Figure 3C, Supplementary Table 1C; n=4-7 repeats each). Thus, hiPSC OPCs could be identified and isolated at different stages of lineage restriction, which were serially represented by A2B5, CD140a, CD9 and O4. Selection based on these epitopes permits the isolation of relatively pure populations of hiPSC-OPCs, while removing residual undifferentiated cells from the isolate.

hiPSC-derived oligodendrocytes generated MBP in contact with human axons in vitro

We next sought to examine the ability of hiPSC oligodendrocytes to myelinate axons in vitro. hiPSC OPCs from each cell line were co-cultured with human fetal cortical neurons isolated from 20 week g.a. fetal brain using PSA-NCAM-directed selection (Windrem et al., 2008). The neurons were cultured on laminin for 10-14 days to allow phenotypic maturation and fiber extension, and were confirmed free of tissue-derived oligodendrocytes by O4 immunolabeling. hiPSC OPCs were then prepared as clusters of 50-100 μm in diameter, and co-cultured with the fetal neurons for 4 weeks; the cultures were then immunolabeled for MBP and neurofilament (NF). Confocal imaging revealed abundant MBP^+ processes that contacted axons and initiated ensheathment (Figures 2H-J), though unambiguous myelin formation was not noted at the time points imaged. Thus, to better assess myelinogenesis by hiPSC OPCs, we next evaluated their engraftment and myelination in vivo.

hiPSC OPCs efficiently and functionally myelinated the shiverer brain

To definitively establish the myelination competence of hiPSC OPCs, we transplanted them into newborn homozygous shiverer (*shi/shi*) × rag2$^{-/-}$ immunodeficient mice. For this experiment, the mice were implanted with 100,000 hiPSC-derived OPCs bilaterally into corpus callosum (n=4-7 mice/hiPSC line, for K04, C27 and C14 hiPSC-derived OPCs), using previously described methods(Windrem et al., 2008). At 3 or 4.5 months of age, the mice were killed and their brains analyzed in terms of donor cell distribution and density, myelin production and the proportion of myelinated axons, and nodal reconstitution. All 3 of the hiPSC line-derived OPCs were able to robustly myelinate the recipient brains; from each line, high donor cell densities and widespread dispersal were observed throughout the forebrain white matter (Figures 4A-B). C27, C14 and K04 hiPSC OPC-derived oligodendrocytic differentiation and myelination were analogous in extent, with robust myelination of the corpus callosum and capsules (Figures 4C, E, and H; Figures 5B, G, and J). As a result of the superior initial neuralization of these 2 lines relative to C14, we achieved higher net yields of OPCs with C27 and K04 hiPSCs, and hence only pursued quantitative assessment of myelination in recipients of C27 or K04 hiPSC OPCs.

Quantitative histology revealed that within the corpus callosa of 3 month (13 week)-old shiverer recipients, C27 and K04 hiPSC-derived OPCs and oligodendroglia, defined as hNA^{+}/OLIG2^{+}, achieved densities of 29,498 ± 13,144 and 37,032 ± 8392 cells/mm^3, respectively. Among these, 7,298 ± 2659 (C27) and 2,328 ± 650 (K04) cells/mm^3 expressed MBP; these comprised 10.9 ± 5.1% (C27) and 4.7 ± 1.1% (K04) of all donor cells within the sampled midline of the corpus callosum, at the 13 week timepoint. To assess the myelination efficiency in terms of the proportion of axons myelinated, we next used confocal analysis to quantify the fraction of callosal axons ensheathed by hiPSC oligodendroglia in the 3 mice engrafted with C27 hiPSC-derived OPCs. At the 13-week time-point analyzed, 17.2 ± 7.2% of host mouse axons were ensheathed within the three sampled callosa (Figure 5B). Remarkably, the density of hiPSC-OPC donor-derived myelination, and the proportion of ensheathed axons at 13 weeks, proved as high as, and perhaps exceeded, that achieved by OPCs derived from second trimester fetal brain tissue, whether isolated as A2B5^{+}/PSA-NCAM^{-} or CD140a^{+} cells (Sim et al., 2011; Windrem et al., 2004; Windrem et al., 2008).

hiPSC OPCs efficiently generated astrocytes as well as oligodendrocytes in vivo

Besides the large numbers of hiPSC OPCs that differentiated as myelinogenic oligodendrocytes in the shiverer mouse brain, large numbers also remained as resident OLIG2^{+} and NG2^{+} progenitor cells, while many OPCs of all 3 hiPSC lines differentiated as astrocytes as well, particularly so as fibrous astrocytes of the white matter (Figures 4D, F and I). When hiPSC OPC transplanted mice were assessed at 13 weeks after neonatal graft, most donor cells persisted as progenitors or had initiated oligodendroglial differentiation; by that timepoint, the net proportion of OLIG2^{+} cells, which included both OPCs and oligodendroglia, arising from all K08 and C27 transplanted cells was 78.7 ± 2.4%, while the remainder were largely donor-derived GFAP^{+} astroglia (Supplementary Table 2).

Interestingly, despite the widespread infiltration of the recipient brains by hiPSC OPCs, substantial astrocytic differentiation was noted by those cells within the presumptive white matter, within which the donor cells differentiated as morphologically apparent fibrous astrocytes, in close association with hiPSC-derived oligodendrocytes. These hiPSC-derived astrocytes might have been generated from lineage-restricted hiPSC-derived astrogliogenic precursors, or by astrocytic differentiation in situ, from still-bipotential hOPCs. In either case, by 3 months post-neonatal transplant, the callosal and capsular white matter of shiverer recipients of OPC grafts derived from all 3 hiPSC lines manifested human astrocytic scaffolds harboring densely engrafted myelinogenic oligodendrocytes, in each case yielding

substantially reconstructed and densely myelinated central white matter (Figures 4D, F and I).

Neonatal engraftment with hiPSC OPCs could rescue the shiverer mouse

We next asked whether the robust engraftment and myelination noted in transplanted shiverer mice was sufficient to ameliorate neurological deterioration and prolong the survival of shiverer mice, which typically die by 20 weeks of age. To this end, we transplanted a set of 22 neonatal homozygous shiverer × rag2 nulls with 300,000 C27-derived hiPSC OPCs, using a 5-site forebrain and brainstem injection protocol that achieves whole-neuraxis engraftment by transplanted OPCs (Figures 6A-D)(Windrem et al., 2008). A matched set of 19 littermate controls were injected only with saline, and both sets were housed without further manipulation. Predictably, the 19 unimplanted shiverer controls died before 5 months of age, with a median survival of 141 days. In contrast, 19 of the 22 implanted mice lived longer than the longest-lived control mouse. The transplanted mice exhibited greatly prolonged survival (Figure 6E), with reduced death over our 9-month period of observation, at which point the experiment was terminated so that surviving mice could be processed for both immunohistochemical assessment of late-stage myelination and nodal reconstitution, and for ultrastructural analysis (see below). Comparison of the Kaplan-Meier survival plots of transplanted and control mice proved revealed that they were highly significantly different (chi-squared = 17.95 by Gehan-Breslow-Wilcoxon test; $p<0.0001$) (Figure 6E). Those transplanted mice that survived beyond 6 months uniformly exhibited substantial myelination of the brain, brainstem and cerebellum (Figures 6A-D and S3). Remarkably, the timepoint-matched degree of cerebral myelination, as well as the proportion of shiverers alive at any given time-point, were greater in hiPSC OPC-engrafted mice than in mice previously engrafted with fetal human tissue-derived A2B5-sorted OPCs (Windrem et al., 2008), which had been otherwise treated identically.

hiPSC OPCs generated ultrastructurally mature myelin with nodal reconstitution

In light of the markedly extended survival of hiPSC OPC-transplanted mice, we next sought to confirm that this was associated with the formation of ultrastructurally compact myelin around host axons by hiPSC oligodendrocytes. To this end, we used electron microscopy on samples of corpus callosum derived from 22-36 week-old engrafted shiverers (n=3); these mice comprised animals that had been subjected to the 5-site injection protocol, and survived significantly longer than their unengrafted controls; these apparently rescued mice were killed after relatively long survival time points, so as to permit assessment of their myelin integrity and quality. We found that their recipient callosa were densely myelinated, by mature compact myelin characterized by concentrically organized major dense lines (Figures 7A-E) and interlaminar tight junctions (Figures 7F-G and S4C); the engrafted callosa were quite unlike their untransplanted shiverer controls, which failed to exhibit major dense lines or any other evidence of myelin compaction (Figures S4B, D-E).

Anatomic reconstitution of nodes of Ranvier was also noted in these mice, as determined by immunolabeling of Caspr and ßIV-spectrin, which respectively identified paranodal and nodal segments of newly-myelinated axons (Figures 7H-I). In past studies, we correlated the anatomic and antigenic reconstitution of nodal architecture with the restoration of both rapid conduction and functional competence (Windrem et al., 2008). The rapid and robust re-acquisition of nodal architecture in these mice suggests that hiPSC-derived oligodendrocytes generate the cues necessary for the nodal organization of axonal proteins, upon which the formation of functional nodes of Ranvier depends.

Together, these data indicate that hiPSC-derived OPCs can efficiently generate oligodendrocytes, which in turn can robustly myelinate the hypomyelinated shiverer

forebrain, and that the myelin thereby generated is able to restore nodal architecture as well as to ensheath axons as efficiently as purified isolates of fetal tissue-derived OPCs.

hiPSC OPCs were non-tumorigenic in vivo

The persistence of undifferentiated pluripotent stem cells may cause either teratomas or neuroepithelial tumors in graft recipients (Roy et al., 2006). To assess if any pluripotent or incompletely-differentiated hESCs or hiPSCs remained in nominally fully-differentiated oligodendrocyte cultures, we used both immunolabeling and qRT-PCR to assess the expression of pluripotential markers by late stage hiPSC-derived OPCs. By 100 DIV, no detectable OCT4, NANOG or SSEA4 protein could be found in OPCs derived from any of the hESC and hiPSC lines used in this study. Similarly, qRT-PCR revealed that transcripts of OCT4 and human telomerase reverse transcriptase (hTERT) were down-regulated to essentially undetectable levels by DIV 95 or older (Figure S2J-K). We also examined the in vivo expression of OCT4, NANOG, and SSEA4 by engrafted OPCs, 3-months after transplantation. As noted, only a small minority of hNA^{+} donor cells was unstained by OLIG2, MBP or GFAP. Many donor-derived cells expressed nestin or SOX2, suggesting their persistence as neural progenitors; but no persistent expression of OCT4, NANOG, or SSEA4 was detectable in any of these cells, from any of the lines assessed.

Accordingly, we found no evidence of teratoma formation in any of the 16 shi/shi × $rag2^{-/-}$ mice examined for this purpose, which included mice transplanted neonatally with 100,000 cells and killed either 3 (n=11), 4.5 (n=5) months later. We also examined available mice in our survival series, all of whom had been transplanted at 5 sites with a total of 300,000 cells, and died between 4 and 9 months of age (n=10); none had any evidence of teratomas, heterotopias or any type of tumor formation. In addition, we transplanted hiPS cells into normally-myelinated rag2-null mice, so as to assess tumorigenicity in the wild-type myelin environment as well. Of 5 mice examined 6 months after transplantation, none showed any evidence of tumor formation or heterotopias, or even foci of undifferentiated expansion. Of note, persistent expression of SOX2, KLF4, and c-MYC mRNA was noted by qPCR in the hiPSC-derived cells, reflecting some level of unsilenced expression of the lentivirally-inserted reprogramming genes; nonetheless, the expression of the these transcripts was not associated with tumorigenesis by cells transplanted at the end of stage 6.

The lack of tumor formation in hiPSC OPC-engrafted mice was associated with a significant fall in the mitotic fraction of the implanted hiPSC OPCs, as a function of time after graft. hiPSC OPC proliferation *in vivo*; this was measured as Ki67 expression by all human donor cells, which was noted to decrease linearly from 3 months (13.6 ± 0.6%) to 6 months (4.3 ± 0.04%) of age (R^2=0.9; P=0.001; n=7).

To establish the role of our differentiation protocol in diminishing the risk of tumorigenesis, we also transplanted rag2 null mice with both C27 and K04 hiPSCs at the end of stages 1 and 3. This was also done as a positive control for tumor detection, given our lack of observed tumors in the hiPSC OPC (stage 6) engrafted mice, as far out as 9 months after transplant. Yet in contrast to the hiPSC OPC-engrafted mice, which were entirely tumor-free, *every* animal engrafted with earlier stage hiPSCs manifested histologically overt tumor formation by 3 months (n=8 mice engrafted with stage 1 hiPSCs; n=6 with stage 3 cells). Thus, our differentiation protocol appeared to effectively deplete the donor cell pool of persistent undifferentiated cells; the resultant grafts of hiPSC OPCs proved uniformly non-tumorigenic when studied as long as 9 months after transplant.

DISCUSSION

In this study, we established the feasibility of using human induced pluripotential stem cells (iPS cells) to generate highly enriched populations of both astrocytes and myelinogenic central oligodendrocytes, with high efficiency and yield. The success of our protocol in all 4 lines used in this study, which includes WA9/H9 hES cells as well as K04, C14 and C27 iPSCs, suggests its broad applicability, while the high efficiency gliogenesis afforded by this strategy indicates its robust nature. Most importantly, the robust myelination that we noted in vivo, which compared favorably to that previously demonstrated by tissue-derived fetal human glial progenitors, suggested the likely functional integration and utility of these grafts. Accordingly, we noted that myelination-deficient shiverers engrafted neonatally with hiPSC OPCs survived significantly and substantially longer than did both their untransplanted and saline-injected controls; indeed, over three fourths of hiPSC OPC-transplanted mice survived over 6 months, long after all untreated control mice had died. As a result, we can now reliably produce hiPSC OPCs from single patient skin samples, in sufficient numbers to provide myelinogenic autografts, largely – though perhaps not completely (Zhao et al., 2011) - free of rejection risk.

Importantly, the myelination efficiency of the implanted iPSC-derived OPCs, defined as the proportion of central axons myelinated as a function of time after graft, proved as high as that which we had previously achieved using tissue-derived, CD140a-sorted OPCs (Sim et al., 2011). Indeed, it was remarkable to note that the proportion of axons ensheathed was as high in enriched but unsorted hiPSC OPC grafts, as in fetal tissue-derived OPC grafts that had been sorted for $CD140a^+$ cells prior to transplant. Indeed, the hiPSC-OPCs grafts myelinated more axons more rapidly than did A2B5/PSA-NCAM-sorted fetal tissue-derived cells, likely reflecting the higher proportion of bipotential glial progenitor cells in the hiPSC OPC populations by the time of their harvest and transplantation.

In light of the robust myelination afforded by hiPSC OPC grafts, we asked whether neonatal transplantation of hiPSC OPCs might be sufficient to rescue the phenotype and survival of recipient shiverer homozygotes, as we had previously observed in a minority of shiverers transplanted with fetal human brain-derived OPCs. We found that the hiPSC OPC-transplanted mice indeed exhibited markedly improved survival, with both delayed and overall reduced death in the transplanted group over the 9-month period of observation. As we had previously documented with fetal brain tissue-derived OPC grants, the rescued mice manifested progressive resolution of their neurological deficits (Windrem et al., 2008). Remarkably though, the proportion of animals whose survival benefitted from hiPSC OPC transplantation was substantially higher than that which we previously reported using tissue-derived human OPCs: whereas we had observed that only a quarter of shiverer mice transplanted with tissue-derived OPCs survived beyond 6 months of age (Windrem et al., 2008), in our present study over half of hiPSC OPC-engrafted mice did so (Figure 6E). Nonetheless, some later deaths beyond 7 months of age were still noted; this may have reflected an inhomogeneous dispersal of hiPSC OPCs, the nature of which we continue to investigate, that we observed in some animals. Those late deaths notwithstanding, at least a fifth of the mice appeared to represent outright clinical rescues, though we sacrificed these survivors at ≥9 months for histological and ultrastructural analysis. These provocative data suggest the superiority of the hiPSC OPCs as therapeutic vectors, perhaps by virtue of their more rapid myelinogenesis, which may be a function of the prolonged differentiation conditions that we employed in our OPC induction protocol.

Interestingly, we observed no evidence of tumorigenesis from implanted hiPSC-derived glial progenitors, at time points as long as 9 months after transplant. This was surprising, as previous studies had provided ample evidence for the risk of tumor formation from either

residual undifferentiated cells (Pruszak et al., 2009), or from partially differentiated neuroepithelial cells in hES-derived transplants (Roy et al., 2006). It is possible that the prolonged differentiation protocols that we employed to produce OPCs are so robust as to effectively eliminate any residual undifferentiated cells prior to transplantation. It is similarly possible that epigenetic marks persisting in reprogrammed hiPSCs effectively lowered the later risk of tumorigenesis by their differentiated derivatives. In any case, even longer survival time points will be needed, with more animals and an intensive search for any residual undifferentiated and/or potentially tumorigenic cells in vivo, before we can confidently state the safety of these grafts. Should tumorigenesis at any point be a concern, then hiPSC OPCs may be sorted to purity before transplantation, based upon the high incidence of definitively pro-oligodendrocytic $CD9^+/CD140a^+$ cells in our cultures, and our ability to isolate these cells by FACS based upon these co-expressed epitopes (Sim et al., 2011).

These findings indicate that high efficiency in vivo oligodendrocytic differentiation and myelination can be achieved from hiPS cells, suggesting the potential utility of iPS-derived autografts in treating acquired disorders of myelin. Yet it is also important to note the efficient, context-dependent generation of both fibrous and protoplasmic astrocytes from engrafted hiPSC OPCs. Besides the importance of astroglia in effecting the structural and physiological reconstitution of dysmyelinated tracts, astrocytic engraftment may be of especial importance in correcting dysmyelinating disorders of enzyme deficiency, since astrocytic lysosomal enzymes have been found to readily transit from wild-type to deficient glia within brain tissue, sufficiently so to potentially rescue enzyme deficient hosts (Lee et al., 2007). In addition, hiPSC-derived astrocytes may prove critically important therapeutic vectors for diseases of primarily astrocytic pathology (Krencik et al.), such as Alexander Disease and the vanishing white matter disorders (Bugiani et al., 2011), in which myelin loss occurs but may be secondary to astrocytic dysfunction. In each of these cases though, the therapeutic use of iPSC-derived astroglia will need to be paired with methods for the ex vivo correction of the genetic defects characteristic of these disorders.

Human iPSC OPCs might thus be attractive vectors for restoring or replacing glial populations in a variety of disease settings. Most critically, our data suggest the preferential use of hiPSC-derived OPCs to restore lost myelin in disorders such as multiple sclerosis and traumatic demyelination, in which no genetic abnormalities might complicate the use of a patient's own somatic cells as iPS source. iPSC OPCs may similarly prove of great therapeutic value in genetic disorders of myelin, such as Pelizaeus-Merzbacher Disease, recognizing that the underlying genetic defect must first be repaired in the donor somatic cells, before glial progenitor induction and implantation. Our present study thus establishes the technical feasibility and efficacy of generating myelinogenic oligodendrocytes from hiPS cells, and suggests the clinical situations in which this approach might be most appropriate. We may now reasonably contemplate the clinical application of patient-specific, somatic cell-derived glial progenitor cell transplants for the treatment of the acquired disorders of myelin, as well as of the broader spectrum of human glial pathologies.

EXPERIMENTAL PROCEDURES

hESC and hiPSCs culture

We used 4 distinct lines of pluripotential cells in this study. These included hESCs (WA09/H9; WiCell, Madison, Wisconsin), and human iPS cells (hiPSCs) of both keratinocyte (K04; K. Hochedlinger) and fibroblast origin (C14 and C27 hiPSCs; L. Studer). The experiments described were approved by the University of Rochester Embryonic Stem Cell Research Oversight committee.

Oligodendrocyte progenitor cell production

OPCs were induced from hES and iPS cells using our modifications of published protocols (Hu et al., 2009a; Hu et al., 2009b; Izrael et al., 2007a), as schematized in Figure 1, and described in detail in the Supplemental Methods.

Directed astrocytic or oligodendrocytic maturation

hiPSC- or hESC-derived gliogenic spheres at 120-170 DIV were cultured in suspension in GIM supplemented with PDGF-AA (10 ng/ml), IGF-1 (10 ng/ml) and NT3 (10 ng/ml). To differentiate these OPCs into mature OLs or astrocytes, the spheres were dissected into small cell clusters (around 50-100 μm diameter) mechanically with a Sharpoint blade (Surgimed MLB, Inc.). The dissected OPC clusters were plated onto poly-ornithine/laminin coated 12-well plates and cultured in GIM for 1-2 weeks. For induction of astrocytes, the OPC clusters were cultured either in GIM supplemented with PDGF-AA (10 ng/ml), IGF-1 (10 ng/ml) and NT3 (10 ng/ml) or in GIM supplemented with 10% fetal bovine serum (FBS, Hyclone) for 1-2 weeks. For directing the maturation of OLs, the cultures were switched to half GIM supplemented with PDGF-AA (5 ng/ml), IGF-1 (5 ng/ml) and NT3 (5 ng/ml) plus half Neurobasal Media (NB, Invitrogen) supplemented with B27 (1X) and BDNF (10 ng/ml) and grown for 2-4 weeks. The mature astrocytes were recognized with immunostaining of anti-GFAP or anti-CD44. Oligodendroglia were identified using anti-O4 and anti-MBP antibodies.

In vitro immunocytochemistry

All in vitro fixation and immunolabeling protocols are detailed in the Supplemental Methods.

Isolation of human fetal neuronal progenitor cells for co-culture

Human fetal forebrain tissue was obtained from second-trimester aborted fetuses of 20 weeks gestational age (g.a.). Tissues were obtained as de-identified tissue, as approved by the Research Subjects Review Board of the University of Rochester Medical Center. The tissue samples were washed 2-3 times with sterile Hank's balanced salt solution with Ca^{++}/Mg^{++} ($HBSS^{+/+}$). Cortical plate (CTX) tissue was separated from the ventricular zone/subventricular zone (VZ/SVZ), then dissociated with papain (Worthington Biochemical) as described (Keyoung et al., 2001), (Wang et al., 2010). The cells were resuspended at 2-4 × 10^6 cells/ml in DMEM/F12 supplemented with N2 and bFGF (20 ng/ml) and plated in suspension culture dishes. A day later, the cells were recovered and neurons isolated by magnetic activated cell sorting (MACS) (Windrem et al., 2008). Briefly, the recovered neural progenitor cells were incubated with PSA-NCAM (Chemicon) at 1:100 for 30 min, then washed and labeled with rat anti-mouse IgM microbeads (Miltenyi Biotech). The bound PSA-$NCAM^+$ neurons were eluted, spun, washed with DMEM/F12, then cultured in DMEM/F12 with N2, 0.5% PD-FBS and bFGF (20 ng/ml) for 4-6 days. For co-culture with hiPSC OPCs, the fetal cortical neurons were dissociated into single-cells and then plated onto either poly-L-ornithine/laminin coated 24-well plates or poly-L-ornithine/fibronectin coated coverslips (50,000-100,000 cells/well or coverslip). The replated neurons were then switched to Neurobasal media with B27 (1X) and BDNF (10 ng/ml, Invitrogen), for an additional 6-10 days prior to co-culture.

Co-culture of hiPS derived OPCs with human fetal cortical neurons in vitro

Gliogenic OPC spheres derived from either K04- or C27-hiPSCs were induced up to 130 DIV prior to co-culture. These were dissected into small pieces of <1 mm^3 and cultured for 2-3 weeks, to allow the OPCs to expand as a monolayer surrounding the core clusters. The OPC clusters and their monolayer surrounds were then recollected with cold $HBSS^{-/-}$ from

the culture dishes, and manually dissected into smaller fragments of 100-200 μm diameter. Small aliquots were fully dissociated into single cells with Accutase (Chemicon) for 5 min at room temperature, then assessed by hemocytometry. For co-culture, the hiPSC OPCs were then seeded at 200,000 cells/ml, either with or without human cortical neurons, and cultured in a 1:1 mixture of NB/B27/BDNF and GIM/ NT3/IGF1/PDGF-AA media. The cultures of cortical neurons alone, hiPSCs OPCs alone, or both populations together were allowed to grow 2-4 weeks further before fixation and immunolabeling for O4, MBP, GFAP and ßIII-tubulin.

Flow cytometry

Flow cytometric methods, by which hESC- and hiPSC-derived OPCs were analyzed for A2B5, CD140a, CD9 and O4 immunoreactivities, as well as the cell preparation methods antecedent to cytometry and sorting, are described in detail in Supplemental Methods and materials.

RNA extraction and RT-PCR

Total RNA was extracted from undifferentiated hESC and hiPSCs, or hESC- and hiPSC-derived OPCs, using RNeasy mini kit (Qiagen). The first of strand of cDNA was transcribed using Taqman reverse transcription kit (Roche #N808-0234). The primer sequences are given in the Supplementary Methods. The relative abundance of transcript expression of mRNAs was measured by ABI PRISM 7000 system. The resultant expression data were normalized to expression level of glyceraldehyde-3-phosphate dehydrogenase (GAPDH) mRNA. Statistical analysis was performed on transformed data. The means and SEMs were calculated following a paired t test.

Neonatal xenograft into shiverer mice

Homozygous shiverer mice (The Jackson Laboratory, Bar Harbor, ME) were crossed with homozygous rag2 null immunodeficient mice (Shinkai et al., 1992) on the C3H background (Taconic, Germantown, NY) to generate *shi/shi* × $rag2^{-/-}$ myelin-deficient, immunodeficient mice. The hiPSC-derived OPCs were prepared for transplantation as described for in vitro co-culture. Neonatal pups were either transplanted bilaterally in the corpus callosum with a total of 100,000 cells, as described in Windrem, et al., 2004, or with 300,000 cells, using the procedure described in Windrem 2008. At 3 months of age, transplanted mice were anesthetized with pentobarbital, then perfusion fixed with cold $HBSS^{+/+}$ followed by 4% paraformaldehyde. Brains were extracted and post-fixed for 2 hr in cold paraformaldehyde. Brains processed for EM were perfused in 4% paraformaldehyde and 0.25% glutaraldehyde.

Immunohistochemistry of tissue sections

Human cells were identified with mouse anti-human nuclear antigen (hN), clone 235-1 (MAB1281 at 1:800, Millipore, Billerica, MA). Phenotypes were identified with human-specific NG2 (MAB2029 at 1:200, Millipore, Billerica, MA); rat anti-MBP (Ab7349 at 1:25), rabbit anti-OLIG2 (Ab33427 at 1:1000, Abcam, Cambridge, MA), human-specific mouse anti-GFAP (SMI-21 at 1:500), mouse anti-neurofilament (NF, SMI-311 and SMI-312 at 1:1000, Covance, Princeton, NJ), and rabbit anti-Ki67 (RM-9106 at 1:200, Thermo-Fisher, Freemont, CA). Alexa Fluor secondary antibodies, including goat anti-mouse, -rat, and -rabbit antibodies conjugated to 488, 568, 594, and 647 nm fluorophores, were used at 1:400 (Invitrogen, Carlsbad, CA). Antibodies against PAX6, NKX2.2, OCT4, NANOG, and SOX2 were employed using the same conditions as in vitro.

Morphometrics

Myelinated Axon Counts—Regions of dense engraftment with human cells were selected for neurofilament and MBP staining; a 1 μm stack of 10 superimposed optical slices taken at 0.1 μm intervals (Olympus FluoView 300) was made for each of three fields of view in the corpus callosum. Three parallel, equidistant lines were laid over the images perpendicular to the axons. Axons were scored at intersections with the lines as either myelinated (closely apposed to MBP on both sides) or unmyelinated.

Mapping of human cell engraftment—The positions of all anti-human nuclei$^+$ cells were mapped on 20 μm coronal sections at 160 μm intervals from -3.2 to 1.2 bregma AP.

Cell counting—Three unilateral, equally-spaced samples of corpus callosum, from -0.4 to 1.2 bregma, were counted for cells expressing human nuclear antigen together with either MBP, hGFAP, OLIG2, or Ki67. White matter was also assessed for the presence of any human nuclear antigen$^+$ cells co-expressing HuC/D, OCT4, or NANOG. All data are provided as means ± SEM.

Electron microscopy

Samples of human iPSC-derived glial chimeric white matter were taken from mice killed at 22-24 weeks of age, perfused with half-strength Karnovsky's fixative, then processed for ultrastructural analysis of myelin morphology and quality using previously described techniques (Windrem et al., 2008).

Supplementary Material

Refer to Web version on PubMed Central for supplementary material.

Acknowledgments

This work was supported by the New York State Stem Cell Board (NYSTEM), the National Multiple Sclerosis Society, NIH grants R01NS75345, R01NS39559, and R01MH099578, the G. Harold and Leila Y. Mathers Charitable Foundation, and the Dr. Miriam and Sheldon G. Adelson Medical Research Foundation. We thank Karen Bentley and Gayle Schneider for their assistance in electron microscopy.

References

Ben-Hur T, Goldman SA. Prospects of cell therapy for disorders of myelin. Ann N Y Acad Sci. 2008; 1142:218–249. [PubMed: 18990129]

Berry M, Hubbard P, Butt AM. Cytology and lineage of NG2-positive glia. J Neurocytology. 2002; 31:457–467.

Bugiani M, Boor I, van Kollenburg B, Postma N, Polder E, van Berkel C, van Kesteren RE, Windrem MS, Hol EM, Scheper GC, et al. Defective glial maturation in vanishing white matter disease. J Neuropathol Exp Neurol. 2011; 70:69–82. [PubMed: 21157376]

Chambers SM, Fasano CA, Papapetrou EP, Tomishima M, Sadelain M, Studer L. Highly efficient neural conversion of human ES and iPS cells by dual inhibition of SMAD signaling. Nat Biotechnol. 2009; 27:275–280. [PubMed: 19252484]

Dietrich J, Noble M, Mayer-Proschel M. Characterization of A2B5+ glial precursor cells from cryopreserved human fetal brain progenitor cells. Glia. 2002; 40:65–77. [PubMed: 12237844]

Franklin RJM, ffrench-Constant C. Remyelination in the CNS: from biology to therapy. Nat Rev Neurosci. 2008; 9:839–855. [PubMed: 18931697]

Hu BY, Du ZW, Li XJ, Ayala M, Zhang SC. Human oligodendrocytes from embryonic stem cells: conserved SHH signaling networks and divergent FGF effects. Development. 2009a; 136:1443–1452. [PubMed: 19363151]

Hu BY, Du ZW, Zhang SC. Differentiation of human oligodendrocytes from pluripotent stem cells. Nat Protoc. 2009b; 4:1614–1622. [PubMed: 19834476]

Izrael M, Zhang P, Kaufman R, Shinder V, Ella R, Amit M, Itskovitz-Eldor J, Chebath J, Revel M. Human oligodendrocytes derived from embryonic stem cells: Effect of noggin on phenotypic differentiation in vitro and on myelination in vivo. Mol Cell Neurosci. 2007a; 34:310–323. [PubMed: 17196394]

Izrael M, Zhang P, Kaufman R, Shinder V, Ella R, Amit M, Itskovitz-Eldor J, Chebath J, Revel M. Human oligodendrocytes derived from embryonic stem cells: Effect of noggin on phenotypic differentiation in vitro and on myelination in vivo. Mol Cell Neuroscience. 2007b; 34:310–323.

Keirstead HS, Nistor G, Bernal G, Totoiu M, Cloutier F, Sharp K, Steward O. Human embryonic stem cell-derived oligodendrocyte progenitor cell transplants remyelinate and restore locomotion after spinal cord injury. J Neurosci. 2005; 25:4694–4705. [PubMed: 15888645]

Keyoung HM, Goldman SA. Glial progenitor-based repair of demyelinating neurological diseases. Neurosurg Clin NA. 2007; 18:93–104.

Keyoung HM, Roy NS, Benraiss A, Louissaint A Jr, Suzuki A, Hashimoto M, Rashbaum WK, Okano H, Goldman SA. High-yield selection and extraction of two promoter-defined phenotypes of neural stem cells from the fetal human brain. Nat Biotechnol. 2001; 19:843–850. [PubMed: 11533643]

Krencik R, Weick JP, Liu Y, Zhang ZJ, Zhang SC. Specification of transplantable astroglial subtypes from human pluripotent stem cells. Nat Biotechnol. 2011; 29:528–534. [PubMed: 21602806]

Lee J-P, Jeyakumar M, Gonzalez R, Takahashi H, Lee P, park K-I, Butters T, Dwek R, Schwartz P, Tong G, et al. Stem cells act through multiple mechanisms to benefit mice with neurodegenerative metabolic disease. Nature Medicine. 2007; 13:439–447.

Maherali N, Ahfeldt T, Rigamonti A, Utikal J, Cowan C, Hochedlinger K. A high-efficiency system for the generation and study of human induced pluripotent stem cells. Cell Stem Cell. 2008; 3:340–345. [PubMed: 18786420]

Pruszak J, Ludwig W, Blak A, Alavian K, Isacson O. CD15, CD24, and CD29 define a surface biomarker code for neural lineage differentiation of stem cells. Stem Cells. 2009; 27:2928–2940. [PubMed: 19725119]

Qi Y, Cai J, Wu Y, Wu R, Lee J, Fu H, Rao M, Sussel L, Rubenstein J, Qiu M. Control of oligodendrocyte differentiation by the Nkx2.2 homeodomain transcription factor. 2001; 128:2723–2733.

Roy NS, Cleren C, Singh S, Yang L, Beal MF, Goldman SA. Functional engraftment of human ES cell-derived dopaminergic neurons enriched by co-culture with telomerase-immortalized midbrain astrocytes. Nature Medicine. 2006; 12:1259–1268.

Roy NS, Wang S, Harrison-Restelli C, Benraiss A, Fraser RA, Gravel M, Braun PE, Goldman SA. Identification, isolation, and promoter-defined separation of mitotic oligodendrocyte progenitor cells from the adult human subcortical white matter. J Neurosci. 1999; 19:9986–9995. [PubMed: 10559406]

Shinkai Y, Rathbun G, lam K, Oltz E, Stewart V, Mendelsohn M, Charron J, Datta M, Young F, Stall A, et al. RAG2-deficient mice lack mature lymphocytes owing to inability to initiate V(D)J rearrangement. Cell. 1992; 68:855–867. [PubMed: 1547487]

Sim FJ, McClain CR, Schanz SJ, Protack TL, Windrem MS, Goldman SA. CD140a identifies a population of highly myelinogenic, migration-competent and efficiently engrafting human oligodendrocyte progenitor cells. Nat Biotechnol. 2011; 29:934–941. [PubMed: 21947029]

Terada N, Baracskay K, Kinter M, Meltrose S, Brophy P, Boucheix C, Bjartmar C, Kidd G, Trapp B. Then tetraspanin protein CD9 is expressed by progenitor cells committed to oligodendrogenesis and is linked to B1 integrin CD81 and Tspan2. Glia. 2002; 40:350–359. [PubMed: 12420314]

Thomson JA, Itskovitz-Eldor J, Shapiro SS, Waknitz MA, Swiergiel JJ, Marshall VS, Jones JM. Embryonic stem cell lines derived from human blastocysts. Science. 1998; 282:1145–1147. [PubMed: 9804556]

Wang S, Chandler-Militello D, Lu G, Auvergne R, Geschwind D, Coppola G, Nicolis S, Sim F, Goldman SA. Prospective identification, direct isolation, and expression profiling of a telomerase

expressing subpopulation of human neural stem and progenitor cells, using sox2 enhancer-directed, GFP-based FACS. Journal of Neuroscience. 2010 in press.

Windrem MS, Nunes MC, Rashbaum WK, Schwartz TH, Goodman RA, McKhann G, Roy NS, Goldman SA. Fetal and adult human oligodendrocyte progenitor cell isolates myelinate the congenitally dysmyelinated brain. Nature Medicine. 2004; 10:93–97.

Windrem MS, Roy NS, Wang J, Nunes M, Benraiss A, Goodman R, McKhann GM, Goldman SA. Progenitor cells derived from the adult human subcortical white matter disperse and differentiate as oligodendrocytes within demyelinated lesions of the rat brain. J Neurosci Res. 2002; 69:966–975. [PubMed: 12205690]

Windrem MS, Schanz SJ, Guo M, Tian GF, Washco V, Stanwood N, Rasband M, Roy NS, Nedergaard M, Havton LA, et al. Neonatal chimerization with human glial progenitor cells can both remyelinate and rescue the otherwise lethally hypomyelinated shiverer mouse. Cell Stem Cell. 2008; 2:553–565. [PubMed: 18522848]

Zhao T, Zhang ZN, Rong Z, Xu Y. Immunogenicity of induced pluripotent stem cells. Nature. 2011; 474:212–215. [PubMed: 21572395]

Zhou Q, Choi G, Anderson DJ. The bHLH transcription factor Olig2 promotes oligodendrocyte differentiation in collaboration with Nkx2.2. 2001; 31:791–807.

Zhou Q, Wang S, Anderson DJ. Identification of a novel family of oligodendrocyte lineage-specific basic helix-loop-helix transcription factors. 2000; 25:331–343.

Highlights

- Myelinogenic oligodendrocyte progenitor cells (OPCs) were generated from human iPSCs
- hiPSC OPCs myelinated the brains of shiverer mice, and increased their survival
- Myelination by hiPSC OPCs was faster than that of fetal tissue-derived OPCs
- hiPSC OPCs produced both astrocytes and oligodendrocytes, and were non-tumorigenic

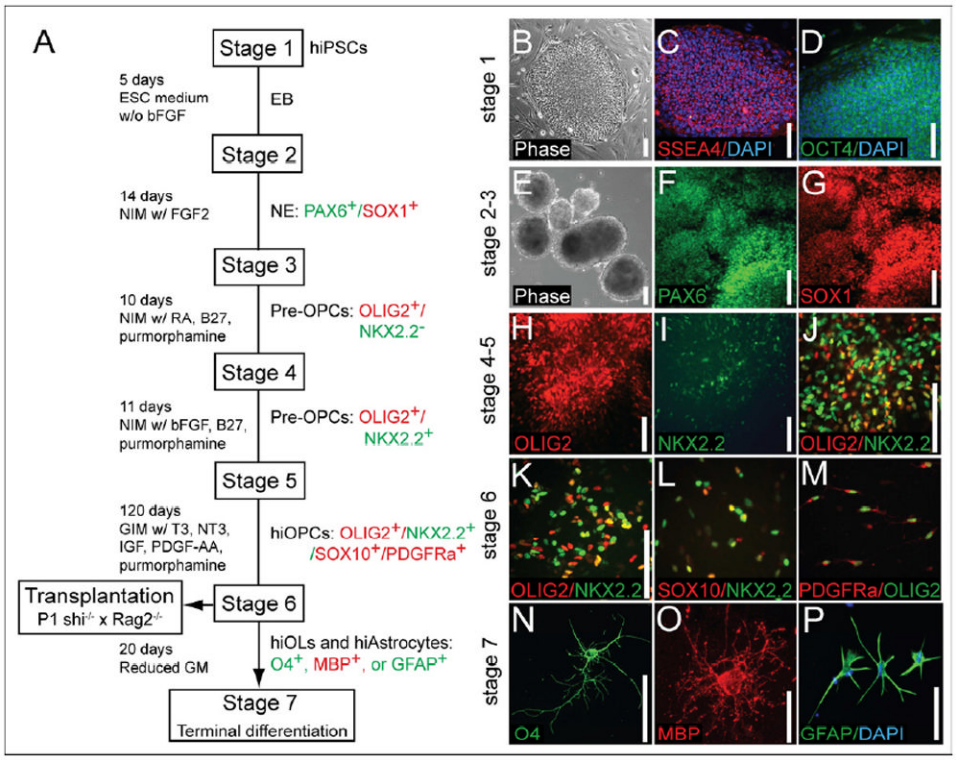

Figure 1. hiPSCs can be directed into OPC fate

(A) A schematic protocol for directed differentiation of hiPSC into OPCs. Embryoid bodies (EBs) were differentiated from undifferentiated hiPSC (Stage 1) from DIV 0-5. EBs were then differentiated as neuroepithelial (NE) cells in neural induction media (NIM; see Methods) with bFGF. **(B-D)** Undifferentiated hiPSCs (stage 1) and hiPSC colonies expressed the pluripotency markers SSEA-4 and OCT4. EBs **(E)** and neuroepithelial cells **(F-G)** could be generated from hiPSC (stages 2-3). hiPSC-derived EBs at this stage expressed the neuroepithelial markers PAX6 and SOX1. **(H-I)** $OLIG2^+/NKX2.2^-$ early GPCs appeared under the influence of RA and purmorphamine, a small molecule agonist of sonic hedgehog signaling. By stage 4, OLIG2 was expressed in early pre-OPCs, which then serially developed NKX2.2 expression. **(J)** $OLIO2^+/NKX2.2^-$ early pre-OPCs were differentiated into later-stage $OLIG2^+/NKX2.2^+$ pre-OPCs, when RA was replaced by bFGF at stage 5. **(K-M)** Pre-OPCs were further differentiated into bipotential OPCs in glial induction media (GIM; see Methods), supplemented with PDGF AA, T3, NT3 and IGF. Stage 6 was extended as long as 3- 4 months, so as to maximize the production of myelinogenic OPCs. By the time of transplant, these cells expressed not only OLIG2 and NKX2.2 **(K)**, but also SOX10 **(L-M)** and PDGFRα **(M)**. By the end of stage 6, hiPSC OPCs could be identified as $OLIG2^+/NKX2.2^+/SOX10^+/PDGFR\alpha^+$. **(N-P)** In vitro terminal differentiation of hiPSC OPCs into human iPSC-derived oligodendrocytes (hiOLs), identified by $O4^+$ **(N)** and MBP^+ **(O)**. Oligodendrocytes and $GFAP^+$ astrocytes **(P)** arose with reduction in glial mitogens.

Scale: **B-N, P**, 100 μm; **O**, 25 μm.

See also Figure S1.

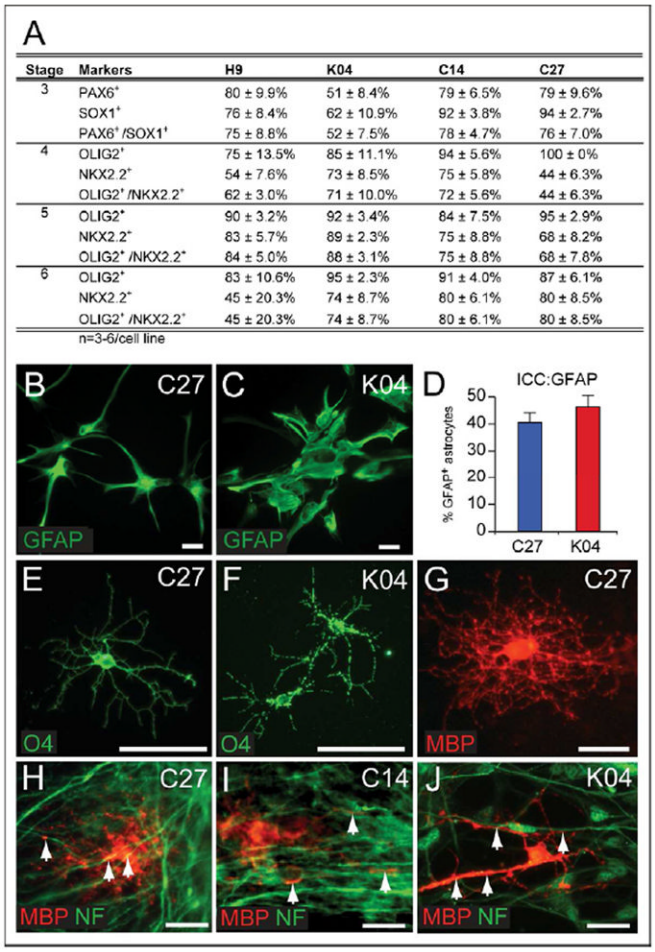

Stage	Markers	H9	K04	C14	C27
3	PAX6$^+$	80 ± 9.9%	51 ± 8.4%	79 ± 6.5%	79 ± 9.6%
	SOX1$^+$	76 ± 8.4%	62 ± 10.9%	92 ± 3.8%	94 ± 2.7%
	PAX6$^+$/SOX1$^+$	75 ± 8.8%	52 ± 7.5%	78 ± 4.7%	76 ± 7.0%
4	OLIG2$^+$	75 ± 13.5%	85 ± 11.1%	94 ± 5.6%	100 ± 0%
	NKX2.2$^+$	54 ± 7.6%	73 ± 8.5%	75 ± 5.8%	44 ± 6.3%
	OLIG2$^+$/NKX2.2$^+$	62 ± 3.0%	71 ± 10.0%	72 ± 5.6%	44 ± 6.3%
5	OLIG2$^+$	90 ± 3.2%	92 ± 3.4%	84 ± 7.5%	95 ± 2.9%
	NKX2.2$^+$	83 ± 5.7%	89 ± 2.3%	75 ± 8.8%	68 ± 8.2%
	OLIG2$^+$/NKX2.2$^+$	84 ± 5.0%	88 ± 3.1%	75 ± 8.8%	68 ± 7.8%
6	OLIG2$^+$	83 ± 10.6%	95 ± 2.3%	91 ± 4.0%	87 ± 6.1%
	NKX2.2$^+$	45 ± 20.3%	74 ± 8.7%	80 ± 6.1%	80 ± 8.5%
	OLIG2$^+$/NKX2.2$^+$	45 ± 20.3%	74 ± 8.7%	80 ± 6.1%	80 ± 8.5%

n=3-6/cell line

Figure 2. Both astrocytes and oligodendrocytes are efficiently generated from hiPSC OPCs

(A) Expression of neural markers during induction of oligodendroglial lineage hiPSC-derived neuroepithelial cells in stage 3, pre-OPCs in stages 4 and 5, and OPCs in stage 6. Cultures were immunostained for Pax6 and Sox1, or Olig2 and Nkx2.2, respectively. The proportion of immunopositive clusters for each marker set were scored, for each hiPSC line. At least 3 repeats in each group were performed; data are provided as means ± SEM. In stage 6, gliogenic clusters were dissociated to single cell suspensions and plated in glial induction media, resulting in the terminal differentiation of both astrocytes and myelinogenic oligodendrocytes. (**B-C**) GFAP$^+$ astrocytes were evident in cultures of hiPSC OPCs by 95 DIV; C27 (**B**) and K04 (**C**) derived astrocytes are shown here. **D**, the proportion of GFAP$^+$ astrocytes among all cultured cells at 95 DIV; the remainder expressed oligodendroglial lineage markers (see Figure S2I). Later in stage 6 **(E-J**, 160 DIV**)**, hiPSC-derived OPCs differentiated as both O4$^+$ (**F-G**) and myelin basic protein (MBP)$^+$ **(G)** oligodendrocytes. (**H-J**) When co-cultured with human fetal cortical neurons, hiPSC OPCs derived from C27 (**H**), C14 (**I**), and K04 (**J**) hiPSCs all generated MBP$^+$ myelinogenic oligodendrocytes that engaged neurofilament$^+$ axons (MBP, *red*; neurofilament, *green*). Scale: 50 μm.

See also Figure S2.

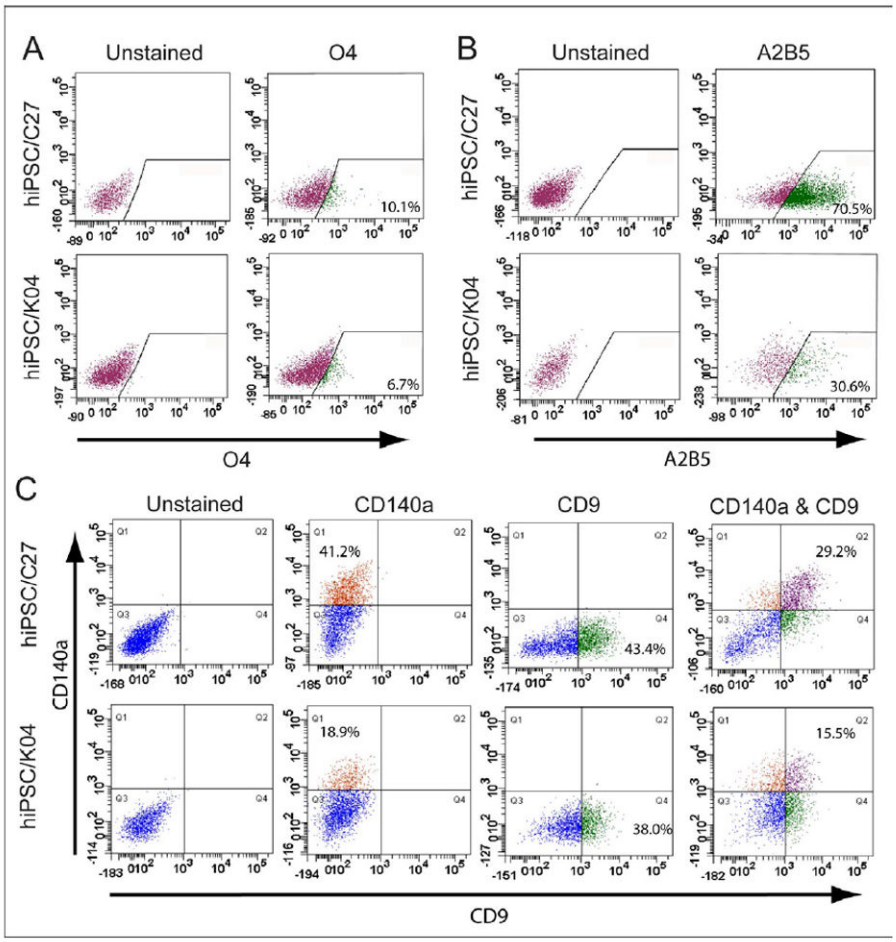

Figure 3. OPCs can be isolated from mixed hiPSC culture by CD140a- and CD9-directed FACS

(A) hiPSC OPC-derived oligodendrocytes were recognized and isolated by fluorescence-activated cell sorting (FACS) using monoclonal antibody O4, which recognizes oligodendrocytic sulfatide. The incidence of $O4^+$ oligodendroglia varied across different hiPSC lines, from 4 to 12% (See Supplementary Table 1; n=4-7 experiments). **(B)** OPCs derived from hiPSCs (C27 and K04) were readily recognized with the cell surface marker A2B5. **(C)** OPCs derived from either hiPSCs (C27 and K04) or hESC (WA09/H9) were readily recognized with cell surface markers, PDGFRα (CD140a) and CD9, by FACS analysis. The relative proportions of CD140a, CD9 and CD140a/CD9 double-labeled cells varied across the different cell line-derived OPCs (n=4-7 experiments).
See also Supplementary Table 1, Tables S1A and S1B.

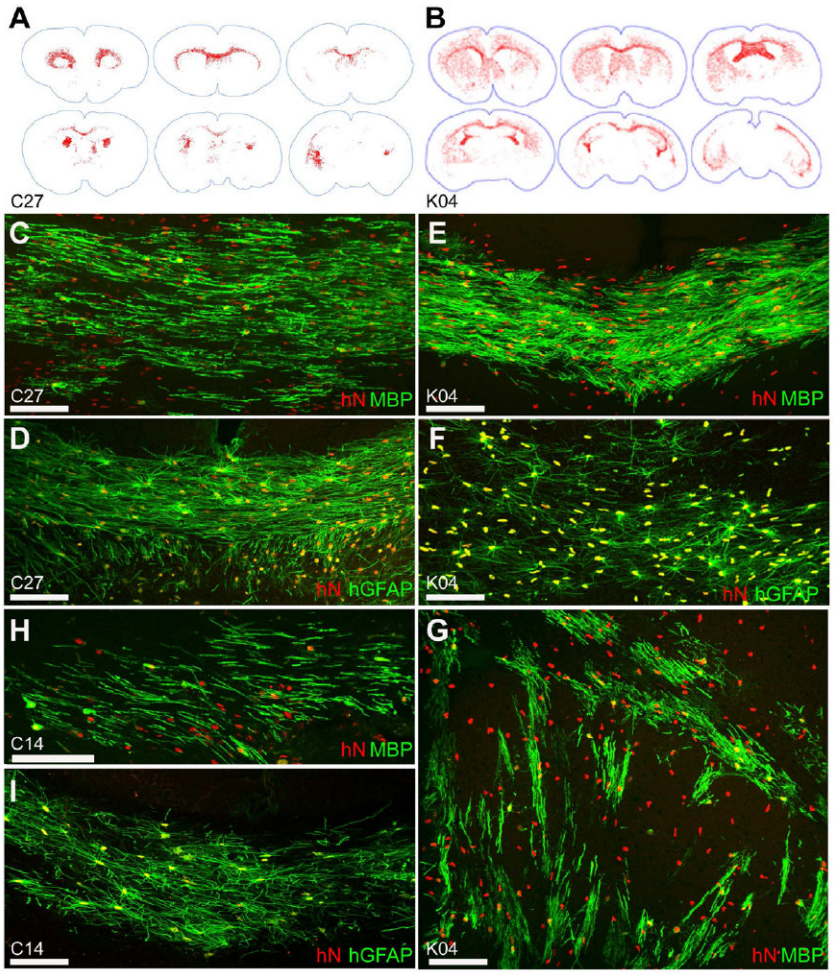

Figure 4. hiPSCs migrate widely and differentiate as astroglia and myelinogenic oligodendrocytes

hiPSC OPCs generated from all 3 hiPSC lines migrated throughout the shiverer brain, engrafting most densely in white matter. Distributions of C27 **(A)** and K04 **(B)** hiPSC-derived OPCs shown (human nuclear antigen $(hNA)^+$, *red*, mapped in Stereo Investigator). By 13 weeks of age, C27 hiPSC OPCs **(C)**, K04 hiPSC OPCs **(E, G)**, and C14 hiPSC OPCs (**H**) matured into myelin basic protein (MBP, *green*)-expressing oligodendroglia throughout the subcortical white matter, including callosal and capsular (**C, E, H**) as well as striatal (**G**) tracts. In these 13 week-old shiverer mouse recipients, C27 **(D)**, K04 **(F)**, and C14 (**I**) hiPSC-derived OPCs also differentiated as astroglia (human-specific GFAP, *green*), especially as fibrous astrocytes in the central white matter.

Scale: **C-I**, 100 μm.

See also Supplementary Table 2.

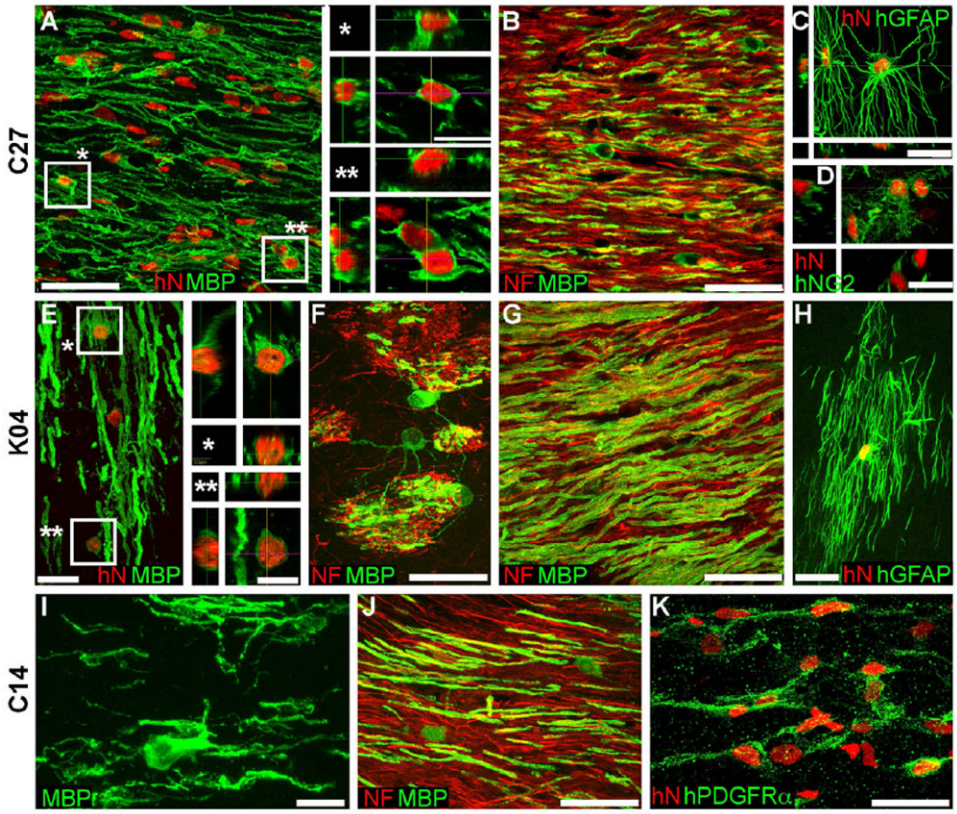

Figure 5. hiPSC OPCs robustly myelinate in vivo

Confocal images of the callosal and capsular white matter of mice engrafted with hiPSC OPCs derived from all 3 tested hiPSC lines demonstrate dense donor-derived myelination. **A-D**, C27-derived; **E-H**, K04; **I-K**, C14.

A, G, and **J** show abundant, donor-derived myelin basic protein expression (MBP, *green*) by C27, K04 and C14 hiPSC OPCs (human nuclear antigen, hNA, *red*), respectively. Representative z-stacks of individual hNA^+ oligodendrocytes are shown as *asterisks* in **A** and **E**. By the 19 week time-point assessed here, C27 (**B**), K04 (**F, G**), and C14 hiPSC oligodendroglia (**J**) robustly myelinated axons (neurofilament, NF, *red*). hiPSC-derived oligodendroglial morphologies exemplified in panels **F** (K04) and **I** (C14); **F** shows multi-axon myelination by single oligodendrocytes in the striatum.

hiPSC OPCs also generated astroglia (**C**, C27; **H**, K04), which exhibited the complex fibrous morphologies typical of human astrocytes (human-specific GFAP, *green*). Many cells also remained as progenitors, immunostaining for NG2 (**D**, C27) and human-specific PDGFαR (**K**, C14).

Scale: **A, B, C, G, J**, 50 μm; **C, D, E, F, H, K**, 20 μm; **I**, 10 μm; insets to **A, E**, 10 μm.

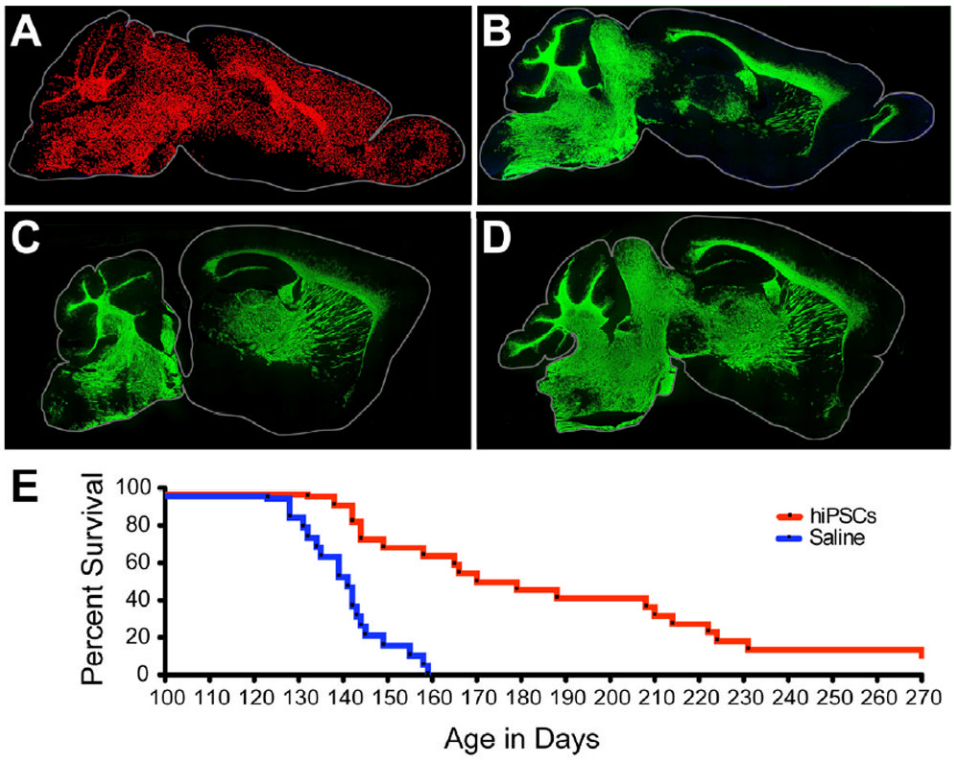

Figure 6. hiPSC OPCs myelinate widely to greatly extend the survival of hypomyelinated mice

A, Dot map indicating distribution of human iPSC-derived donor cells (C27) at 7 months of age, following neonatal engraftment in a shiverer mouse brain. Widespread dispersal and chimerization by hiPSC OPCs is evident (human nuclear antigen, *red*). **B**, hiPSC OPC-derived myelination in shiverer forebrain, at 7 months; section 1 mm lateral to **A**. MBP-immunoreactivity (*green*) is all donor-derived. **C, D**. Myelination in sagittal sections taken at different mediolateral levels from two additional 7 month-old mice, each engrafted with C27 hiPSC OPCs at birth. **E**, Kaplan-Meier plot of survival of C27 iPSC-OPC implanted (n=22) vs. saline-injected (n=19) control mice. Remaining engrafted mice sacrificed for electron microscopy at 9-10 months (≥270 days).

Scale: **A-B**, 2 mm.

See also Figure S3.

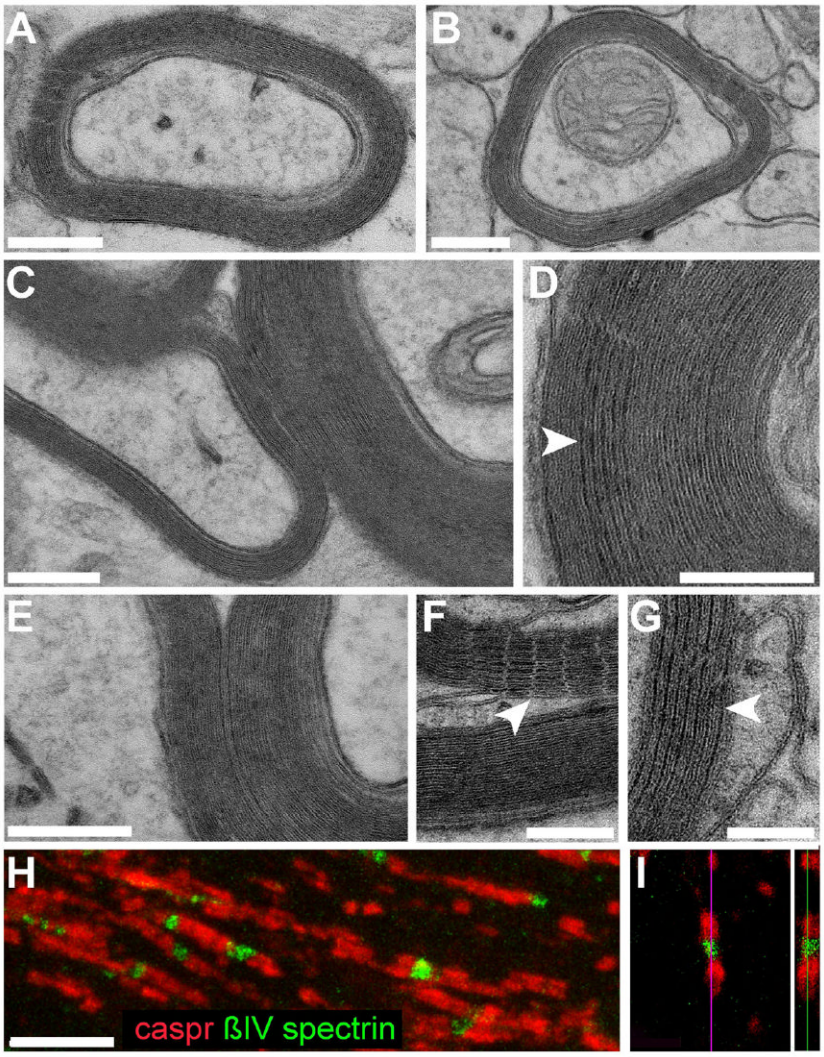

Figure 7. hiPSC-derived oligodendrocytes produce compact myelin and induce nodes of Ranvier

Representative electron microscopic images of sections through the corpus callosum (**A-B**) and ventral pons (**C**) of a 40-week-old shiverer mouse neonatally-engrafted with C27 hiPSC OPCs, showing donor-derived compact myelin with evident major dense lines, ensheathing mouse axons. **D-G** show higher power images of the corpus callosum, also at 40 weeks. **D**, The alternating major dense (*arrowheads*) and intraperiod lines, characteristic of mature myelin, are evident. **F-G**, myelin sheaths in the corpus callosum ensheathing central axons, their maturation manifested by parallel arrays of tight junctions (**F**, *arrowhead*) and major dense lines (**G**, *arrowhead*).

This mature myelination permitted the organization of architecturally-appropriate nodes of Ranvier by hiPSC oligodendroglia. In **H-I**, nodal reconstitution in transplanted shiverers is demonstrated by immunostaining of oligodendrocytic paranodal Caspr protein (*red*), seen flanking nodes of Ranvier identified here by ßIV spectrin (*green*). An isolated node is shown in confocal cross-section in **I**.

Scale: **A-E**, 200 nm; **F-G**, 100 nm; **H-I**, 5 μm.

See also Figure S4.